

THE SECOND INTERNATIONAL VORTEX FLOW EXPERIMENT (VFE-2): RESULTS OF THE FIRST PHASE 2003 - 2008

Dietrich Hummel
Technische Universität Braunschweig

Keywords: *Delta wings, vortical flows, experimental results, CFD results, VFE-2*

Abstract

At the end of the RTO-phase of the Second International Vortex Flow Experiment (VFE-2) the up to now achieved experimental and numerical results on the vortical flow about a delta wing with sharp and blunt leading edges are summarized, and special attention is called to the present status of knowledge. Some problems, which could not be solved within VFE-2, are also mentioned. The needs for further investigations are stressed in an outlook, and the continuation of the research is indicated.

1 Introduction

The First International Vortex Flow Experiment (VFE-1) had been carried out in 1984 to 1986 on a cropped 65° swept delta wing in order to check the CFD codes, which were available at that time [1]. Even for sharp leading edges with fixed primary separation the Euler codes were not well suited to calculate the pressure distribution on a slender wing properly, since the secondary separation is not modelled at all.

In the last fifteen years considerable progress has been achieved in the numerical calculation of vortical flows by taking into account viscous effects through solutions of the RANS equations. This means that Reynolds number effects are now included and secondary vortices turn out. However, for turbulent flows in solutions of the RANS equations a turbulence model is necessary, which has to cover the attached boundary layers and the secondary vortex area properly.

In order to validate the results of Navier-Stokes calculations new and more detailed experimental data were necessary, and therefore at the RTO AVT Symposium in Loen 2001 a Second International Vortex Flow Experiment (VFE-2) has been proposed [2], which will be described subsequently.

2 Nomenclature

A	= aspect ratio of the wing
b	= wing span
b_{loc}	= local span at $x = \text{const.}$
C_p	= pressure coefficient ($C_p = (p - p_\infty)/q_\infty$)
c	= root chord ($c = c_R = c_r$)
\bar{c}	= mean aerodynamic chord
f	= frequency
k	= reduced frequency ($k = f\bar{c} / U_\infty$)
M	= Mach number
PSD	= power spectrum density, (SD = spectrum density)
q_∞	= free stream dynamic pressure
R_{mac}	= Reynolds number, based on the mean aerodynamic chord
U_∞	= free stream velocity
r_{LE}	= streamwise leading edge radius
x, y, z	= body fixed coordinate system, origin at wing apex
u, v, w	= components of the velocity vector
u', v', w'	= fluctuations of the velocity vector
u_{rms}	= root mean square of the fluctuations u'
α	= angle of attack
ξ, η, ζ	= dimensionless coordinates ($\xi = x/c, \eta = y/b_{loc}, \zeta = z/b_{loc}$)
Λ	= leading edge sweep

3 Test configuration

The configuration for VFE-2 has been chosen in such a way that all flow regimes (i.e attached flow, separated vortical flow without and with vortex breakdown and separated deadwater-type flow) are covered properly, and this lead again to a delta wing with 65° leading edge sweep.

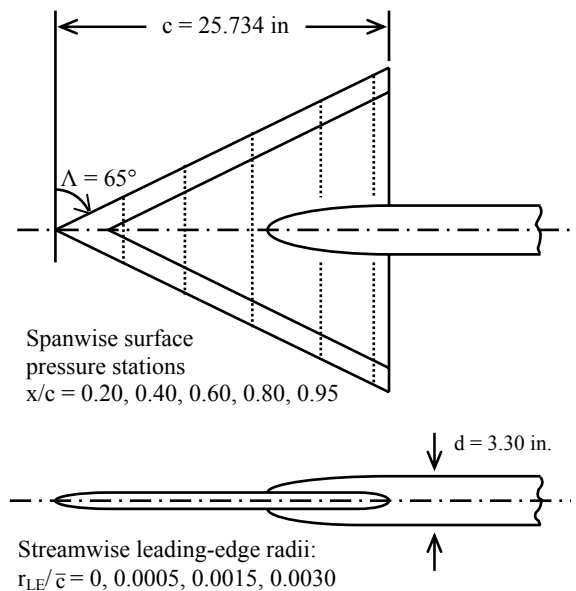


Fig. 1: VFE-2 configuration: NASA NTF delta wing, $\Lambda = 1.85$, $\Lambda = 65^\circ$ [3].

Concerning the thickness distribution a flat plate inner portion in combination with interchangeable leading edges was desired, and these requirements were fulfilled by the NASA configuration [3], which is shown in Figure 1. Sets of one sharp and three rounded leading edges were available. The geometry of the wing as well as the shape of the sting were given by analytical expressions described in all details in [3]. New wind tunnel models could be built quite easily and overall aerodynamic coefficients and pressure distributions in certain cross sections were already available for a large variety of Reynolds numbers and Mach numbers [3], [4].

4 Program of Work

The first phase of VFE-2 has been carried out in 2003 to 2008 within the framework of an RTO Task Group AVT-113 “Understanding and Modelling Vortical Flows to Improve the

Technology Readiness Level for Military Aircraft”. New experimental investigations were performed on various wind tunnel models, see Table 1:

Model 1 was on loan from NASA, USA, (Aerodynamic coefficients and PSI provided). It has been tested at DLR Goettingen, Germany, (PSP and PIV) and at ONERA Lille, France, (Forces and moments, PIV).

Model 2 has been built at TU Munich, Germany, (PIV and hot-wire investigations of the flow field). It has been tested also at DLR Cologne, Germany, under cryogenic conditions (PIV, Laminar/turbulent transition, IR and TSP).

Model 3 has been built at Glasgow University, UK, (Unsteady force and pressure measurements at high angles of attack).

Models 4 and 5 (Sharp and rounded LE) have been built at ONERA Lille, France, (Forces and moments, pressure distributions, flow visualization, PIV). They were also tested at TUBITAK-SAGE Ankara, Turkey, (Forces and moments, laminar/turbulent transition).

The experimental investigations were accompanied by numerical calculations of the flow on structured and unstructured grids by the partners.

Mod. Nr.	Span [m]	Root chord [m]	Leading edge	Tested at	Owner
0	0.610	0.653	S, RS, RM, RL	NASA, NTF	NASA Langley RC
1	0.457	0.490	S, RS, RM, RL	NASA, LTPT DLR, TWG ONERA	NASA Langley RC
2	0.933	0.980	S, RM	TU Munich DLR, KKK	TU Munich
3	0.987	1.059	S, RM	Uni. Glasgow	Uni. Glasgow
4	0.457	0.490	S	ONERA TUBITAK-SAGE	ONERA Lille
5	0.457	0.490	RM	ONERA TUBITAK-SAGE	ONERA Lille

Tab. 1: Wind tunnel models used in VFE-2. [Notations for leading edge shapes: (S) Sharp edged, (RS) Rounded: Small radius, (RM) Rounded: Medium radius, (RL) Rounded: Large radius]

For delta wings with sharp leading edges and fixed primary separation a large number of experimental investigations are available in the literature. Therefore it was decided to use the case of sharp leading edges within VFE-2 as reference only and to direct the main emphasis for new experiments towards studies of the vortex formation on the configuration with rounded leading edges. Since no investigations on the flow field around this configuration existed at all, the main general aim for VFE-2 was to provide flow field data by means of modern measurement techniques for comparison with numerical results. From the proposal for VFE-2 [2] a huge number of interesting flow cases for the 65° delta wing configuration can be deduced. From the very beginning the members of the Task Group realized that not all interesting flow phenomena could be treated successfully and that a concentration concerning the topics to be investigated was necessary.

Most of the new measurements have been carried out for incompressible flows. The available NASA data [3] showed for the configurations with rounded leading edges at medium angles of attack spanwise pressure distributions with two separate suction peaks on the upper surface of the wing, which have never been observed for sharp edged delta wings. Therefore the Task Group decided to study the onset of separated flow for rounded leading edges in more details, and for this purpose the medium radius leading edge configuration ($r_{LE}/\bar{c} = 0.0015$) has been selected. Regarding the angles of attack to be investigated a concentration on certain flow regimes was necessary, and finally the following test program has been carried out:

- Onset of vortical flow, $\alpha = 13^\circ$
 - Sharp leading edges: Separated flow
 - Medium radius leading edges: Partly attached, partly separated flow
- Separated flow without vortex breakdown, $\alpha = 18^\circ$
 - Sharp leading edges
 - Medium radius leading edges
- Separated flow with vortex breakdown, $\alpha = 23^\circ$
 - Sharp leading edges
 - Medium radius leading edges.

5 Results

5.1 Partly separated vortical flows

In this section the results for the medium radius rounded leading edge configuration at *angle of attack* $\alpha = 13^\circ$ are discussed. In this case partly separated flow is present on the upper surface of the wing [4] as sketched in Figure 2. This is the most challenging flow situation both experimentally and numerically.

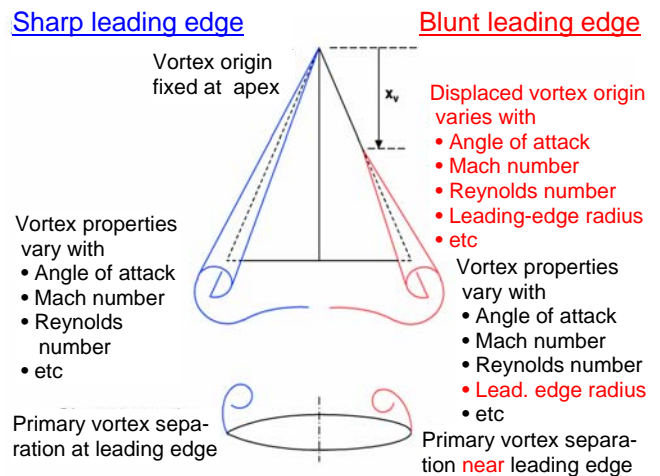


Fig. 2: Comparison of vortical flow features for sharp and blunt leading edge delta wings according to [3].

Results of the PSP investigations from DLR Goettingen on model 1 [7] are shown in Figure 3. In the front part the flow is attached, and in the rear part a vortical flow is established, which is associated with two suction areas on the wing. The stronger outer one was identified to be due to a leading edge vortex, but the inner one could not be understood so easily.

Numerical calculations have been carried out at EADS Munich for this case and according to Figure 4 two co-rotating vortices on each side of the configuration with corresponding suction peaks turned out [13]. Surprisingly the inner vortex was as large as the outer one as shown in Figure 5. The outer vortex is fed with vorticity up to the trailing edge, whereas the inner one decays downstream more and more.

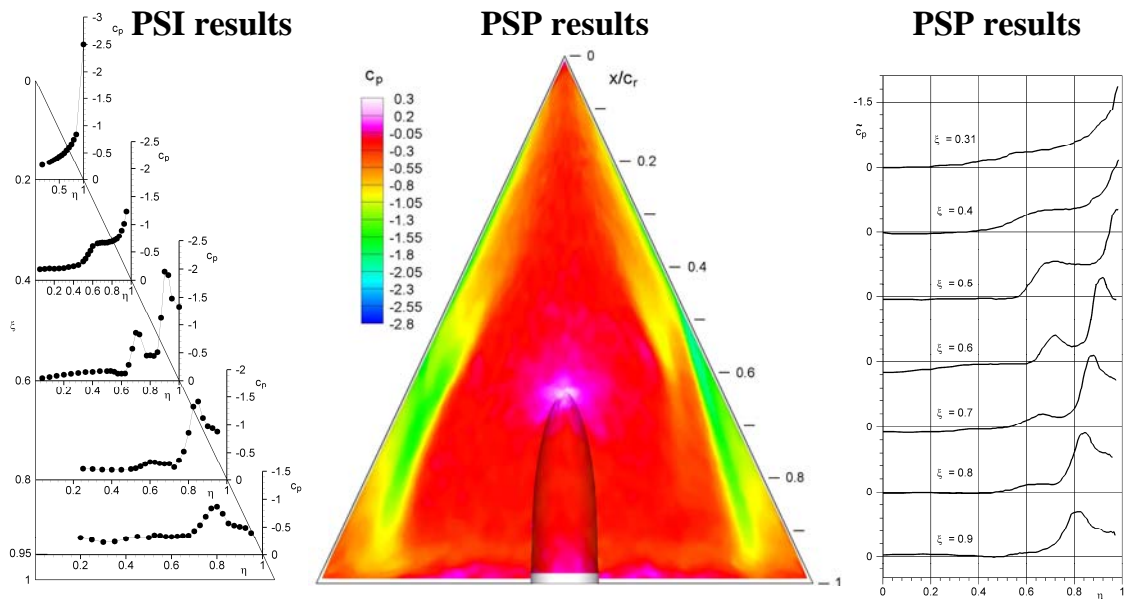


Fig. 3: Experimental pressure distribution on the VFE-2 configuration with medium radius rounded leading edges for $M = 0.4$, $R_{\text{mac}} = 3 \cdot 10^6$, $\alpha = 13^\circ$ [7].

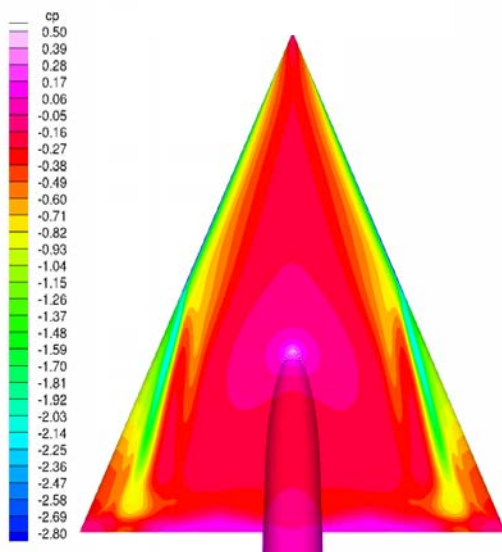


Fig. 4: Numerical pressure distribution on the VFE-2 configuration with medium radius rounded leading edge for $M = 0.4$, $R_{\text{mac}} = 3 \cdot 10^6$, $\alpha = 13^\circ$ [13].

The numerical results came up just after the PSP measurements at DLR Goettingen and they have been used as a guideline for the opti-

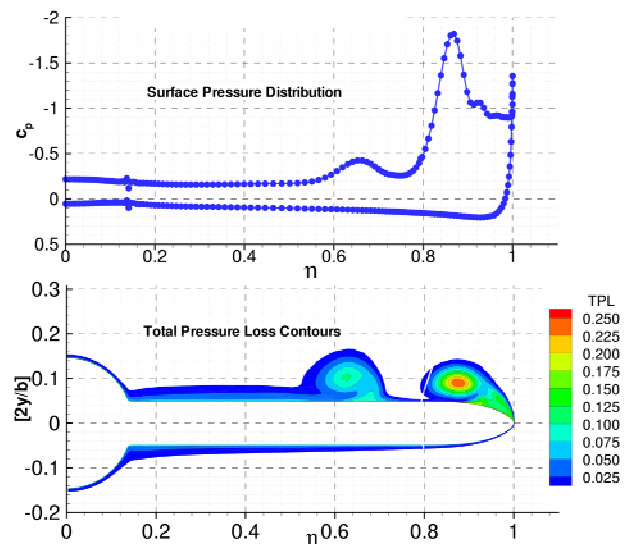


Fig. 5: Numerical vortex pattern in the cross section at $x/c = 0.75$ for the VFE-2 configuration with medium radius rounded leading edge for $M = 0.4$, $R_{\text{mac}} = 3 \cdot 10^6$, $\alpha = 13^\circ$ [13]

cal setup for the subsequent PIV investigations. The results according to Figure 6 show excellent agreement with the numerical findings.

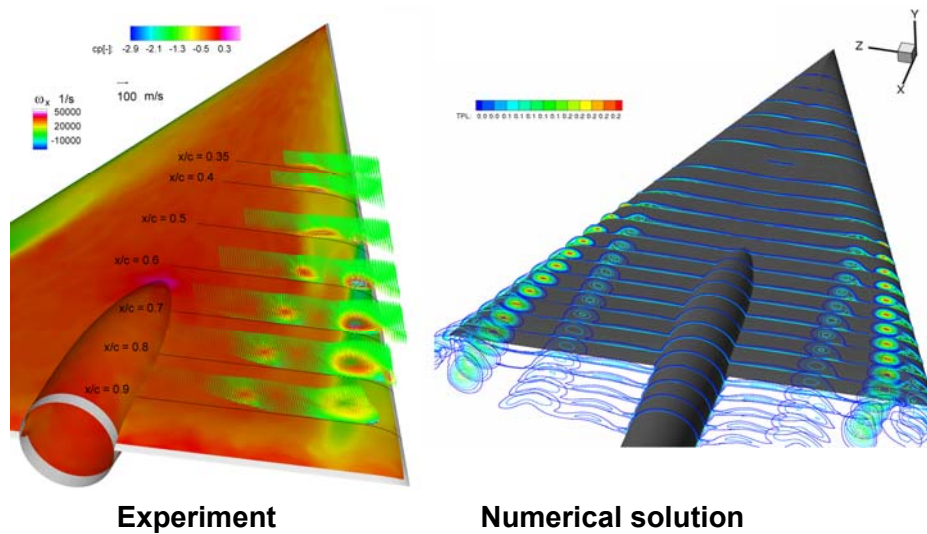


Fig. 6: Pressure (surface colour), velocity (vectors), and vorticity (vector colour) distributions above the VFE-2 configuration with medium radius rounded leading edges for $M = 0.4$, $R_{\text{mac}} = 3 \cdot 10^6$, $\alpha = 13^\circ$. Comparison of the PSP and PIV measurements at DLR [7] with the numerical solution of EADS Munich [13].

In the course of VFE-2 the effects of angle of attack, of Reynolds number and of Mach number have been studied intensively by wind tunnel experiments and by the application of all available CFD solutions on structured and unstructured grids. Details may be taken from the comprehensive presentation of these VFE-2 results at the AIAA Aerospace Sciences Meeting 2008 [5 - 19].

The effect of angle of attack is demonstrated in Figure 7 in combination with Figure 3.

Up to $\alpha = 11.2^\circ$ only the inner primary vortex exists, and the corresponding suction on the wing surface reaches considerable values near the trailing edge. With increasing angle of attack the outer primary vortex is formed in the rear part of the configuration, see Figure 3, and its onset point moves upstream with increasing angle of attack. The strength of the inner primary vortex increases up to the region of the onset of the outer primary vortex, but then decreases suddenly downstream towards the

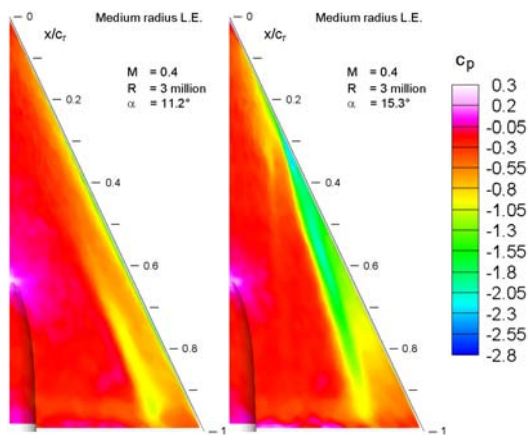


Fig. 7: Pressure distributions on the VFE-2 configuration with medium radius rounded leading edges for $M = 0.4$, $R_{\text{mac}} = 3 \cdot 10^6$ at various angles of attack [7]

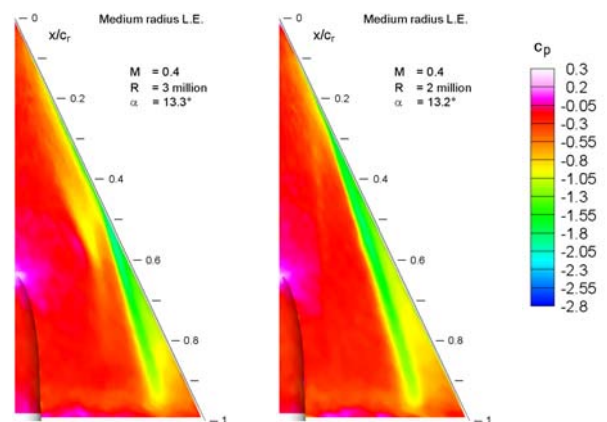


Fig. 8: Pressure distributions on the VFE-2 configuration with medium radius rounded leading edges $M = 0.4$, $\alpha = 13^\circ$ at different Reynolds numbers [7]

trailing edge. This is due to the fact that the vorticity shed from the leading edge is now fed into the outer primary vortex, and this leads to the considerable reduction of the strength of the inner primary vortex. Another effect can also be recognized from Figures 3 and 7: In that region where an outer primary vortex already exists, the weakened inner primary vortex moves distinctly inboard [11].

The vortex formation strongly depends on the Reynolds number [7]. An example is shown in Figure 8. With decreasing Reynolds number the onset of the outer primary vortex moves upstream and its strength increases, whereas the inner primary vortex is weakened and its position moves inboard. Thus, a reduction in Reynolds number has an analogous effect as an increase of the angle of attack according to Figure 7, but nevertheless the reasons for this upstream movement of the onset of the outer primary vortex are different for both cases. With increasing angle of attack the adverse pressure gradients on the upper surface of the wing increase as well, and this leads to the upstream movement of the onset of the outer primary vortex. If the angle of attack is unchanged, however, the adverse pressure gradients remain at the same level, but with decreasing Reynolds number the viscous flow is no longer able to

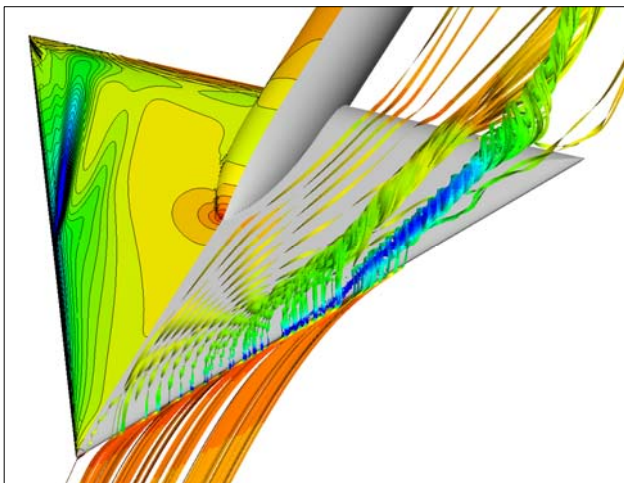


Fig. 9: Numerical solution on a structured grid for the flow around the VFE-2 configuration with medium radius rounded leading edges at $M = 0.4$, $R_{\text{mac}} = 3 \cdot 10^6$, $\alpha = 13.3^\circ$. Pressure distribution (left) and streamlines in the flow field (right) [13].

stay attached, and this leads again to an upstream movement of the onset of the outer primary vortex [11].

Due to the encouraging agreement between the experimental and the calculated results related to the two co-rotating primary vortices, studies of the details of the vortex formation may also be carried out through an analysis of numerical solutions. However, caution is necessary in such an attempt, since the CFD codes themselves are presently not fully validated. The

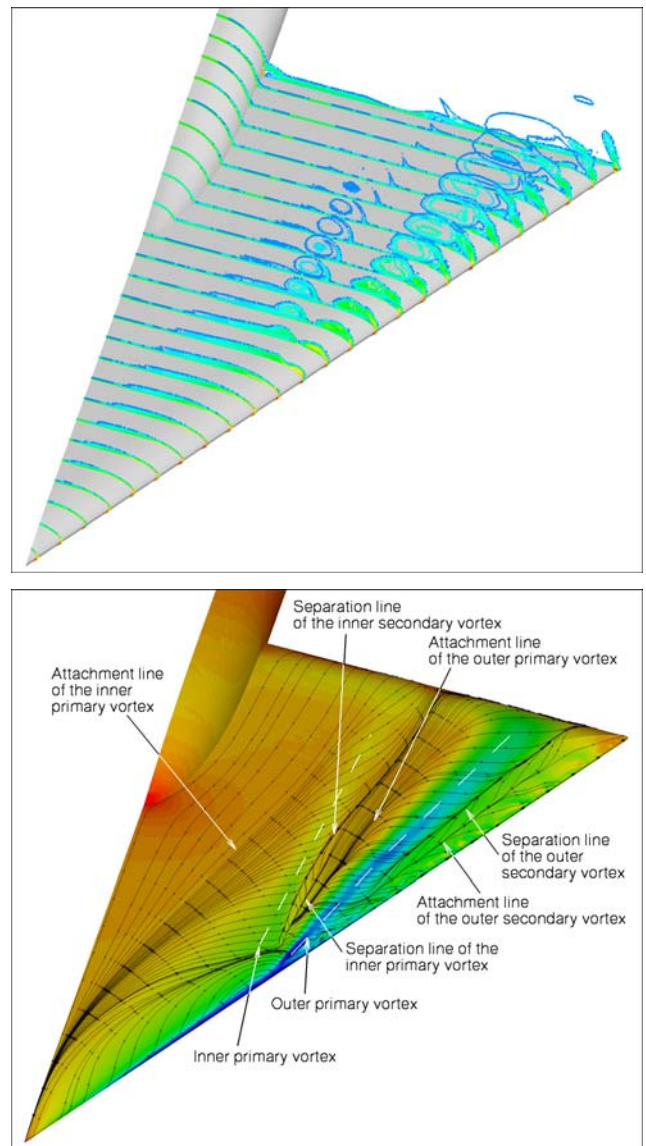


Fig. 10: Numerical solution on an unstructured grid for the flow around the VFE-2 configuration with medium radius rounded leading edges at $M = 0.4$, $R_{\text{mac}} = 3 \cdot 10^6$, $\alpha = 13.3^\circ$. Distribution of axial vorticity (top) and upper surface skin friction lines (bottom) [18].

Figures 9 and 10 show latest calculated results on a structured grid by EADS Munich [13] and on an unstructured grid by DLR Braunschweig [18], and from these numerical results some conclusions may be drawn, which are outlined subsequently and sketched in Figure 11.

The first separation due to the thickness distribution of the configuration takes place near the wing apex. The corresponding separation and attachment lines are located far inboard, and according to experimental results [7], the separated region is thin and broad. According to Figure 10 (top) vorticity is distributed over the whole separated region [18], but a concentrated vortex is not yet present. Underneath the attached flow around the leading edge the outer primary separation develops, and a tiny vortex is formed, marked in both numerical solutions in blue, see Figures 9 and 10 (bottom). Due to this small primary vortex the already existing inner flow separation is now set in a certain order: The vorticity suddenly concentrates and the inner

separation takes the form of an inner primary vortex in the same region where also the outer primary vortex is established. As long as the strength of the outer primary vortex is smaller than that of the inner primary vortex, an attachment line related to the outer vortex and a separation line related to the inner vortex do exist separately. Due to the increasing strength of the outer primary vortex, however, the two lines join and form a cross flow stagnation point, which leaves the wing surface, and correspondingly the outer primary vortex becomes double branched as sketched in Figure 11, and the two vortices are now connected. More downstream the outer primary vortex becomes dominant. Therefore the free stagnation point in the cross flow between the two vortices approaches the wing again, and on the surface it splits up into a separation line corresponding to the inner primary vortex and into an attachment line corresponding to the outer primary vortex. Both vortices are now separated from each other. In this discussion on the conjecturable flow behaviour the secondary vortices related to both primary vortices have not been taken into account, but they could be included into the topology according to Figure 11 quite easily.

With increasing angle of attack the outer primary vortex onset moves upstream. Simultaneously the inner primary vortex weakens more and more and finally disappears for $\alpha \geq 18^\circ$.

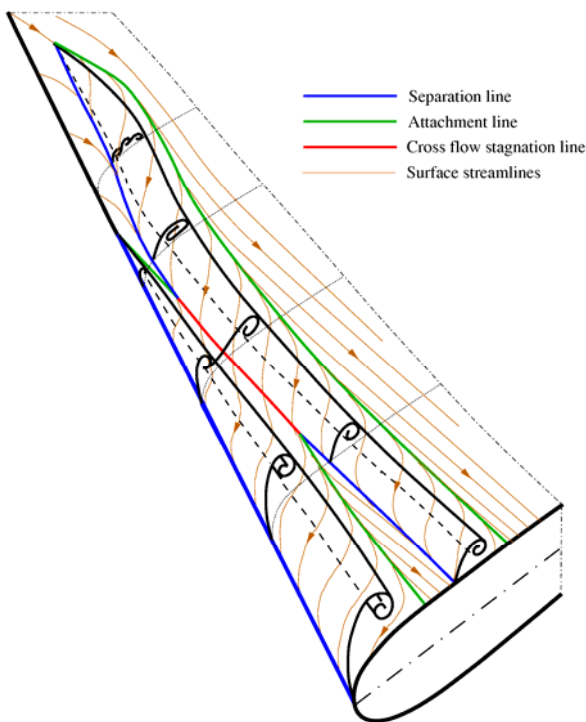


Fig. 11: Schematic view of the vortex formation on the VFE-2 configuration with rounded leading edge at $M = 0.4$, $R_{mac} = 3 \cdot 10^6$, $\alpha = 13.3^\circ$ according to the numerical solutions [13] and [18].

5.2 Fully separated flow without vortex breakdown

In this section the results for the medium radius rounded leading edge configuration at *angle of attack* $\alpha = 18^\circ$ are discussed. For sharp and medium radius rounded leading edges the flow is fully separated along the whole leading edge. This is the standard case of a vortical flow around this configuration.

In almost all experimental contributions to VFE-2 [7 – 9] the time-averaged flow field has been measured using PIV. An example is shown in Figure 12. The fully developed vortical flow is indicated for both cases, and there are only

minor differences concerning the position of the primary vortex relative to the wing.

In order to provide experimental data for comparison with numerical flow solutions using various turbulence models, the flow field has been measured by Hot-Wire Anemometry (HWA) at TU Munich [9], and the complete field of the velocity fluctuations u' , v' , w' is now available. As an example Figure 13 shows the measured fluctuations of the u -component of the velocity u_{rms}/U_∞ as well as $\overline{u'w'}/U_\infty^2$ in the cross section plane at $x/c = 0.6$ for the configuration with sharp leading edges only. From the full measured field of the fluctuations u' , v' , w' the distributions of the turbulent kinetic energy and of the eddy viscosity in the flow field can be determined, and corresponding evaluations of the experiments are still under way.

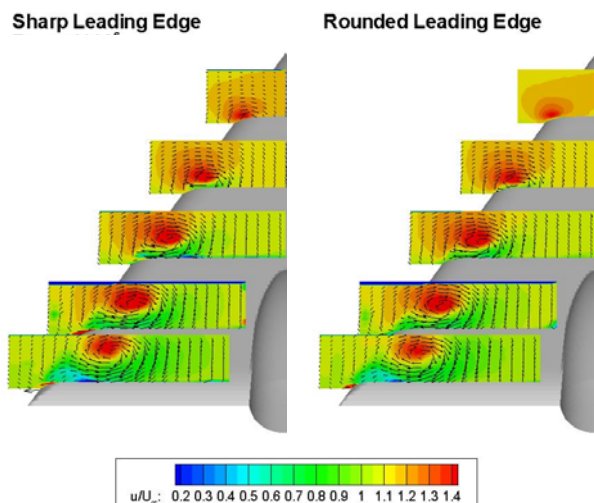


Fig. 12: Flow field around the VFE-2 configuration with sharp and medium radius rounded leading edges at $M \approx 0.1$, $R_{\text{mac}} = 1 \cdot 10^6$, $\alpha = 18^\circ$. PIV results for the time-averaged velocity in various cross sections [9].

Measurements of this kind are also available for the flow conditions at angles of attack $\alpha = 13^\circ$ (section 5.1) and $\alpha = 23^\circ$ (section 5.3). In all cases cross sections at $x/c = 0.4$, 0.6 and 0.8 have been considered. The comparison with CFD solutions using various turbulence models, however, is still pending due to the convergence problems in the numerical solutions for incompressible flows.

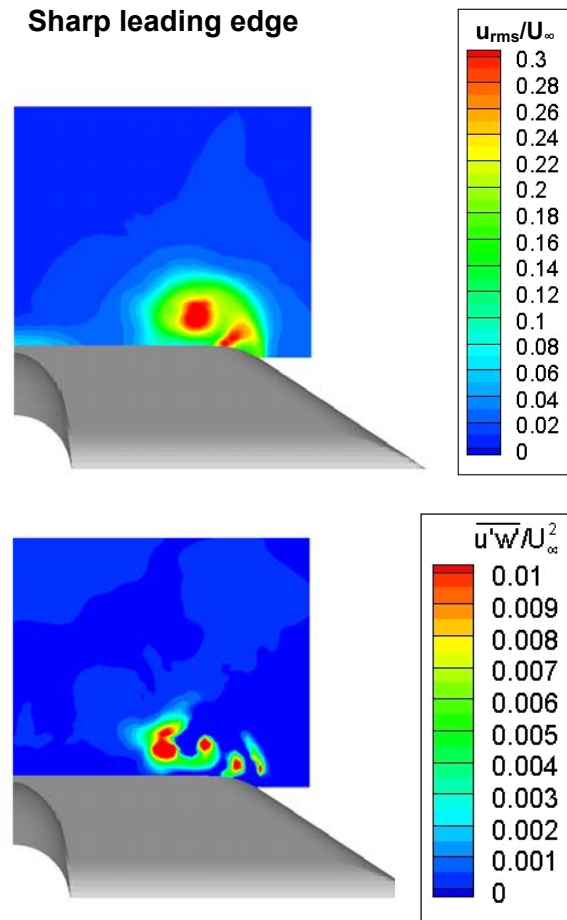


Fig. 13: Flow field around the VFE-2 configuration with sharp leading edges at $M \approx 0.1$, $R_{\text{mac}} = 1 \cdot 10^6$, $\alpha = 18^\circ$. HWA results [9] for the velocity fluctuations u_{rms}/U_∞ and $\overline{u'w'}/U_\infty^2$ in the plane at $x/c = 0.6$.

5.3 Fully separated flow with vortex breakdown

In this section the results for the medium radius rounded leading edge configuration at *angle of attack* $\alpha = 23^\circ$ are discussed. In this case the flow is fully separated and vortex breakdown takes place in the rear part of the wing. Today it is common understanding that the flow past slender delta wings at large angles of attack becomes unsteady even for fixed wings. This means that for large angles of attack and steady boundary conditions only unsteady solutions of the governing equations do exist. The spiral-type vortex breakdown is well predicted by numerical solutions of the Navier-Stokes equations [19], see Figure 14: The instantaneous

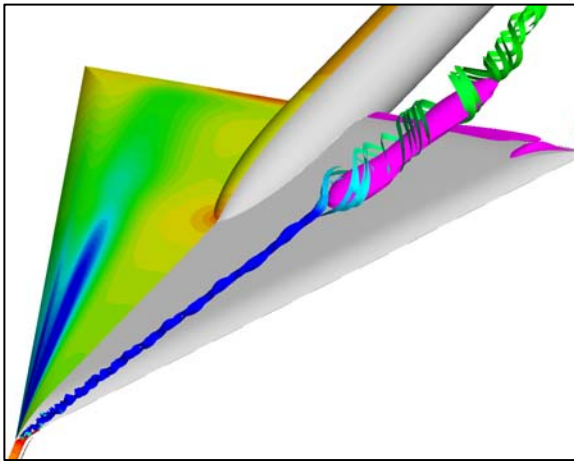


Fig. 14: Numerical simulation of the flow around the VFE-2 configuration with sharp leading edges for $M = 0.4$, $R_{\text{mac}} = 6 \cdot 10^6$, $\alpha = 23^\circ$ [19]. Surface pressure distribution (left) and flow field (right).

vortex axis spirals in space against the sense of rotation of the primary vortex and this spiral turns around with respect to time in the sense of rotation of the primary vortex, and in the centre of the spiraling motion a region of reversed flow is present. Correspondingly all quantities of the flow field show oscillations.

5.3.1 Subsonic flows

In new experiments on the VFE-2 configuration unsteady pressure distribution measurements have been carried out [9] in order to provide data on the oscillations including the governing frequencies for comparison with numerical results. As an example, for the configuration with medium radius rounded leading edges Figure 15 shows the surface pressure fluctuations $(c_p)_{\text{rms}}$ in four cross sections on the wing, and for a certain station in each of these distributions the amplitude spectrum $(SD)_{\text{cp}}$ of the pressure fluctuations as a function of the reduced frequency $k = f\bar{c}/U_\infty$ is given. The high values of the fluctuations around $k \approx 1.3$ in the last section are caused by the spiral motion of vortex breakdown.

For $\alpha = 23^\circ$ flow field measurements in various cross sections have also been carried out at TU Munich [9]. In these cross sections the time-averaged flow field has been measured by means of PIV investigations and the complete

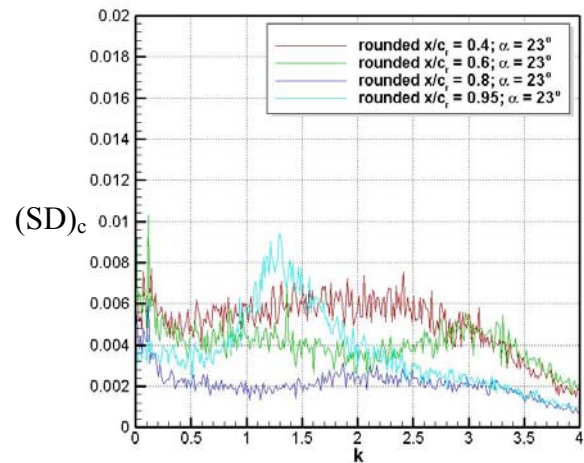
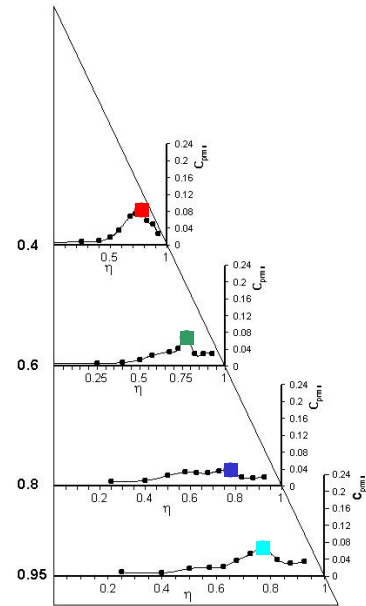


Fig. 15: Surface pressure fluctuations $(c_p)_{\text{rms}}$ on the upper surface of the wing and corresponding spectrum density $(SD)_{\text{cp}}$ for certain stations in four cross sections [9].

unsteady flow field has been determined using the HWA technique. For the configuration with medium radius rounded leading edge Figure 16 shows the unsteadiness of the flow field with vortex breakdown in the cross section at $x/c = 0.8$. The annular form of the area with high fluctuations is typical for the spiral mode of vortex breakdown, and further analysis of these data will lead to experimental results for the frequency of the spiral mode of vortex breakdown. Evaluations of this kind are presently under way.

Rounded leading edge

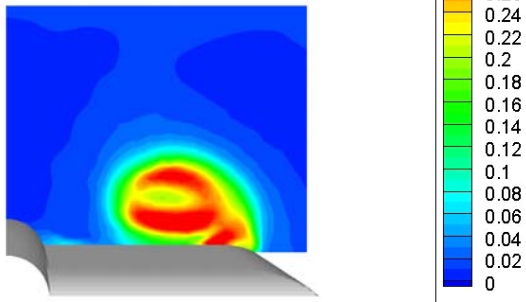


Fig. 16: Flow field around the VFE-2 configuration with medium radius rounded leading edges at $M \approx 0.1$, $R_{\text{mac}} = 1 \cdot 10^6$, $\alpha = 23^\circ$. HWA results [9] for the velocity fluctuations u_{rms}/U_∞ in the cross section at $x/c = 0.8$.

5.3.2 Transonic flows

With increasing Mach number shock waves occur in the vortical flow field. The pressure jumps related to these shocks cause additional unsteadiness in the vortical flow field. Therefore, with increasing Mach number the vortex breakdown onset point is suddenly shifted upstream [7].

The correct prediction of these flow phenomena by CFD codes is very difficult, since the vortical flow field with primary and secondary vortices as well as the strengths of

the embedded shocks must be covered properly in order to get reasonable results as compared with experimental data. A typical result for the present situation is shown in Figure 17. In the EADS solution, which is representative also for other CFD solutions, a strong shock occurs at $x/c_r \approx 0.5$, a dead water type flow is indicated downstream of the shock, and a terminating shock is present at the inner part of the wing. In addition a significant secondary vortex turns out, which also interacts with the shock. The TAI solution, however, shows a much weaker single vortex in the forward part of the wing, which produces obviously a weaker and more downstream positioned shock, and across this shock the suction peak is only slightly reduced. More downstream, at $x/c_r \approx 0.8$, a second weak shock occurs between the wing leading edge and the suction peak area. When reaching the suction peak, this shock wave turns at 90° angle and becomes a weak cross flow shock, which finally merges with the terminating shock close to the trailing edge. This result for the shock formation can also be concluded from the experimental pressure distribution, since the measurements at $x/c_r = 0.8$ and $x/c_r = 0.95$ also give an indication of a weak cross flow shock. This example demonstrates the need for further experimental data on the transonic flow field with vortex breakdown in order to validate the various CFD codes.

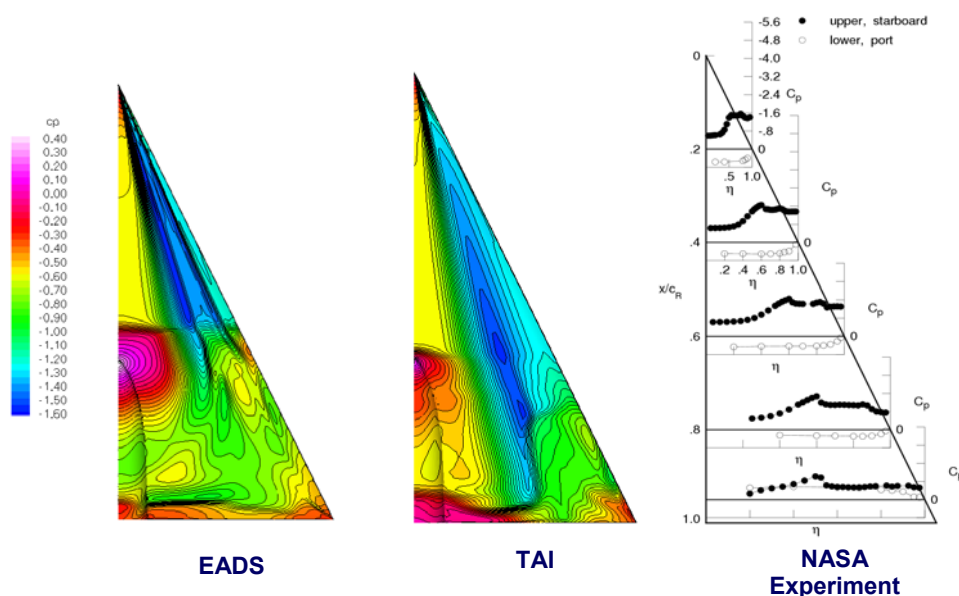


Fig. 17: Surface pressure maps on the VFE-2 configuration with sharp leading edges at $M = 0.85$, $R_{\text{mac}} = 6 \cdot 10^6$, $\alpha = 23^\circ$ [19].

6 Resumé and outlook

In the course of VFE-2 a total of 15 experimental wind tunnel campaigns have been carried out in four countries. The multiple-vortex structure of blunt leading edge separation has been confirmed, and considerably more details of this flow are now available through the use of the Pressure Sensitive Paint (PSP) technique. Detailed flow field measurements by Particle Image Velocimetry (PIV) provided new insight into the vortical structure, and surface and off-body fluctuating measurements by Hot-Wire Anemometry (HWA) showed the turbulent structure of these flows.

Within VFE-2 the available CFD codes have been applied to the vortical flow around the relatively simple delta wing configuration with sharp and rounded leading edges. Numerical calculations have been carried out on structured and unstructured grids. The CFD codes have been validated using the experimental data, and the numerical results have been used as guidelines for the set-up of the wind tunnel experiments. Moreover in the final RTO-phase of VFE-2 the numerical results played an important role in the understanding of the flow physics, since the lack of experimental details in some flow regions could be replaced by numerical results. Therefore the present state of knowledge is the outcome of a proper combination of experiments and numerics.

The scientific work of the VFE-2 team has been carried out within the RTO Task Group AVT-113 from 2003 to 2008, and the achieved status of knowledge has been published in various papers [5 - 19] and it is summarized in the present document. As shown in the preceding chapters, many results could be confirmed, but some problems are still unsolved. Therefore, at the end of the RTO-phase of VFE-2 the scientific program is not terminated. As with VFE-1, the scientific work will continue in the next decade: Many problems have not been solved completely or have even been started, and others have not yet been looked at within the framework of the present Task Group. Therefore new experiments will be carried out worldwide in a new open phase of VFE-2. The configuration under

consideration is relatively simple and described analytically, and therefore new wind tunnel models can be built quite easily. Numerical calculations will go on as well, and better results as well as new solutions will be achieved.

The results of the RTO-phase of VFE-2 will be the starting point for future investigations. Some suggestions for the next steps may be given here:

On the *experimental side* the needs are

- Measurements on the boundary layer status laminar/turbulent for the VFE-2 configuration with sharp and rounded leading edges. Fully developed vortical flow without vortex breakdown at $\alpha = 18^\circ$ should be the starting point, and later also partly separated vortical flow at $\alpha = 13^\circ$ could be added. The already existing experimental results will be further evaluated, but there is an urgent need for new measurements.
- Experimental investigations on the shock formation in transonic fully developed vortical flow $\alpha = 23^\circ$ for the VFE-2 configuration with sharp and medium radius rounded leading edges. Subject should be the mutual interference between the terminating and the cross flow shocks on the one hand and vortex breakdown on the other.
- New measurements on the partly separated vortical flow at $\alpha = 13^\circ$. Up to now the structure of the initial flow separation due to the thickness distribution near the apex of the configuration, see Figure 11 is unknown. Numerical simulations [18] have shown vorticity distributions without a dominating concentrated vortex in this area, see Figure 10 (top), whereas experiments [7] indicate some weak longitudinal vortices in this area.

On the *numerical side* the needs are

- New calculations related to the fully developed vortical flow without vortex breakdown at $\alpha = 18^\circ$ for the VFE-2 configuration with sharp and medium radius rounded leading edges in incompressible flow and at very low Reynolds numbers. Converged solutions should be achieved for various turbulence models, and in comparisons with the available results from Hot-Wire-

Anemometry (HWA) [9] the best suitable turbulence model for calculations of vortical flows should be found.

- Attempts should be made to predict the laminar/turbulent transition in fully developed vortical flows without vortex breakdown at $\alpha = 18^\circ$. Starting point could be the sharp edged VFE-2 configuration. For this purpose two steps would be helpful
 - Calculation of the vortical flow for prescribed laminar and turbulent boundary layer regions on the wing as a guess. A converged solution should be achieved. As input experimental results could be used.
 - Point by point stability analysis of the calculated flow field. Based on the results corresponding modification of the original laminar/turbulent transition guess.
- For partly separated vortical flow at $\alpha = 13^\circ$ the CFD codes should be further validated using the already available or new experimental data. The vortical flow field in the vicinity of the onset point of the outer primary vortex should be analysed in detail in order to check the validity of the schematic view presented in Figure 11.

The first RTO-phase of the Second International Vortex Flow Experiment (VFE-2) has been terminated in 2008. A second open phase of VFE-2 starts now. The scientific community is invited to join this project and to start new investigations. Informations on the ongoing research may be taken from the new website www.dlr.de/as/vfe-2.

References

- [1] Drougge G. The international vortex flow experiment for computer code validation. *ICAS-Proceedings Jerusalem 1988*, Vol. 1, pp. XXXV – XLI.
- [2] Hummel D and Redeker G. A new vortex flow experiment for computer code validation. *RTO AVT Symposium "Vortex Flow and High Angle of Attack Aerodynamics"*, Loen, Norway (2001). RTO-MP-069 (I), SYA 8-1 to 8-31, 2003.
- [3] Chu J and Luckring J. M. Experimental surface pressure data obtained on 65° delta wing across Reynolds number and Mach number ranges. NASA TM 4645, 1996.
- [4] Luckring J M. Reynolds number, compressibility, and leading-edge bluntness effects on delta-wing aerodynamics. *ICAS-Proceedings Yokohama 2004*, Paper 4.1.4.
- [5] Hummel D. Review of the Second International Vortex Flow Experiment (VFE-2). AIAA Paper 2008-0377, 2008.
- [6] Luckring J M. Initial experiments and analysis of vortex flow on blunt edged delta wings. AIAA Paper 2008-0378, 2008.
- [7] Konrath R, Klein Ch and Schroeder A. PSP and PIV investigations on the VFE-2 configuration in sub- and transonic flow. AIAA Paper 2008-0379, 2008.
- [8] LeRoy J F Rodriguez O and Kurun S. Experimental and CFD contribution to delta wing vortical flow understanding. AIAA Paper 2008-0380, 2008.
- [9] Furman A and Breitsamter Ch. Turbulent and unsteady flow characteristics of delta wing vortex systems. AIAA Paper 2008-0381, 2008.
- [10] Coton F, Mat S and Galbraith R. Low speed wind tunnel characterization of the VFE-2 wing. AIAA Paper 2008-0382, 2008.
- [11] Luckring J M and Hummel D. What was learned from the new VFE-2 experiments? AIAA Paper 2008-0383, 2008.
- [12] Nangia R K. Semi-empirical prediction of vortex onset and progression on 65° delta wings (RTO-AVT-113, VFE-2 facet). AIAA Paper 2008-0384, 2008.
- [13] Fritz W. Numerical simulation of the peculiar subsonic flow-field about the VFE-2 delta wing with rounded leading edge. AIAA Paper 2008-0393, 2008.
- [14] Gürdamar E, Ortakaya Y, Kaya S and Korkem, B. Some factors influencing the vortical flow structures on delta wings. AIAA Paper 2008-0394, 2008.
- [15] Schiavetta L A, Boelens O J, Crippa S, Cummings R M, Fritz W and Badcock K J. Shock effects on delta wing vortex breakdown. AIAA Paper 2008-0395, 2008.
- [16] Cummings R M and Schütte A. Detached-eddy simulation of the vortical flow field about the VFE-2 delta wing. AIAA Paper 2008-0396, 2008.
- [17] Crippa S and Rizzi A. Steady, subsonic CFD analysis of the VFE-2 configuration and comparison to wind tunnel data. AIAA Paper 2008-0397, 2008.
- [18] Schütte A and Lüdeke H. Numerical investigations on the VFE 2 65° rounded leading edge delta wing using the unstructured DLR-TAU-Code. AIAA Paper 2008-0398, 2008.
- [19] Fritz W and Cummings R M. What was learned from the numerical simulations for the VFE-2? AIAA Paper 2008-0399, 2008.

Copyright Statement

The authors confirm that they, and/or their company or institution, hold copyright on all of the original material included in their paper. They also confirm they have obtained permission, from the copyright holder of any third party material included in their paper, to publish it as part of their paper. The authors grant full permission for the publication and distribution of their paper as part of the ICAS2008 proceedings or as individual off-prints from the proceedings.